A Multiscale Computational Model for Predicting Damage Evolution in Viscoelastic Composites Subjected to Impact Loading

J. N. Reddy
Department of Mechanical Engineering,
Texas A&M University
College Station, Texas 77843-3123
Tel: (979) 690-7153
e-mail: jnreddy@tamu.edu

Grant No. DAAD 19-01-1-0731

Final Technical Report submitted to

U. S. Army Research Office
P.O. Box 12211
Research Triangle Park, NC 27709-2211

January 2005

Report Documentation Page

Form Approved
OMB No. 0704-0188

Public reporting burden for the collection of information is estimated to average 1 hour per response, including the time for reviewing instructions, searching existing data sources, gathering and maintaining the data needed, and completing and reviewing the collection of information. Send comments regarding this burden estimate or any other aspect of this collection of information, including suggestions for reducing this burden, to Washington Headquarters Services, Directorate for Information Operations and Reports, 1215 Jefferson Davis Highway, Suite 1204, Arlington VA 22202-4302. Respondents should be aware that notwithstanding any other provision of law, no person shall be subject to a penalty for failing to comply with a collection of information if it does not display a currently valid OMB control number.

1. REPORT DATE	2. REPORT TYPE	3. DATES COVERED
JAN 2005	**N/A**	**-**

4. TITLE AND SUBTITLE	
A Multiscale Computational Model for Predicting Damage Evolution in Viscoelastic Composites Subjected to Impact Loading	5a. CONTRACT NUMBER
	5b. GRANT NUMBER
	5c. PROGRAM ELEMENT NUMBER
6. AUTHOR(S)	5d. PROJECT NUMBER
	5e. TASK NUMBER
	5f. WORK UNIT NUMBER
7. PERFORMING ORGANIZATION NAME(S) AND ADDRESS(ES) **U.S. Army Research Office P.O. Box 12211 Research Triangle Park, NC 27709-2211**	8. PERFORMING ORGANIZATION REPORT NUMBER
9. SPONSORING/MONITORING AGENCY NAME(S) AND ADDRESS(ES)	10. SPONSOR/MONITOR'S ACRONYM(S)
	11. SPONSOR/MONITOR'S REPORT NUMBER(S)

12. DISTRIBUTION/AVAILABILITY STATEMENT
Approved for public release, distribution unlimited

13. SUPPLEMENTARY NOTES
The original document contains color images.

14. ABSTRACT

15. SUBJECT TERMS

16. SECURITY CLASSIFICATION OF:			17. LIMITATION OF ABSTRACT	18. NUMBER OF PAGES	19a. NAME OF RESPONSIBLE PERSON
a. REPORT	b. ABSTRACT	c. THIS PAGE			
unclassified	**unclassified**	**unclassified**	**UU**	**30**	

Standard Form 298 (Rev. 8-98)
Prescribed by ANSI Std Z39-18

A Multiscale Computational Model for Predicting Damage Evolution in Viscoelastic Composites Subjected to Impact Loading

by

J. N. Reddy
Department of Mechanical Engineering,
Texas A&M University
College Station, Texas 77843-3123
Tel: (979) 690-7153
e-mail: jnreddy@tamu.edu

EXECUTIVE SUMMARY

The objective of the project was to develop a multiscale computational model capable of predicting the evolution of matrix cracking, delamination, and fiber cracking in viscoelastic composite structures subjected to ballistic impact. The model is three dimensional and computational in nature, utilizing the finite element method, and this model is being implemented to the explicit code DYNA3D. Crack growth is simulated via the cohesive zone model currently under development by the author. The cohesive zone model for predicting damage evolution in laminated composite plates is cast within a three dimensional continuum finite element algorithm capable of simulating the evolution of matrix, fiber, and delamination cracking in composite structures subjected to ballistic impact. Cracking on vastly differing length scales is accounted for by employing global-local techniques, with appropriate damage dependent homogenization techniques introduced to bridge the disparate scales. Finally, simplified generic example problems were solved analytically and compared to computational results obtained with the model as a means of model verification. A damage constitutive model for polymer-matrix composite materials was developed and implemented into a commercially available finite element package.

TECHNICAL DISCUSSION

Preliminary Comments

While accurate models have been developed for predicting impact response of metals and ceramics, which are normally crystalline in nature, models have not been developed for polymeric materials, which have the potential to decrease both mass and cost of such strategic defense weapons. This is due to the different physical nature of fracture in polymeric media, as well as the multiple length scales on which this fracture occurs. The first of these is addressed by a micromechanically based viscoelastic cohesive zone model developed by the principal investigator and coworkers, and the second is solved via the multiscale damage dependent algorithm described herein. These two aspects of the research comprise a unique approach to this problem. The cohesive zone model is unlike any others in existence, in that it requires only

well defined experiments at the microscale. The multiscale algorithm utilizes damage dependent homogenization principles for viscoelastic media that have been recently developed by the author and coworkers, an aspect which has not been correctly incorporated by other researchers.

The research was performed in four coordinated steps: 1) solution of microscale problems; 2) development of homogenization schemes for multiscale analyses; 3) construction of local and global damage evolution algorithms; and 4) solution of model demonstration problems. As a part of the effort, a new simplified explicit finite element code is being developed by the principal investigator. This code is identical in general formulation to DYNA3D, but is designed to simplify the code development process, and to streamline the implementation of the newly developed multiscale subroutines directly into DYNA3D. All of these results are included in the Ph.D. dissertation of Cha Searcy, a graduate student who has worked on the project with Dr. David Allen, and they are not reported here.

The results of a damage constitutive model for polymer-matrix composite materials that was developed and implemented into a commercially available finite element package are discussed in this report.

INTRODUCTION

Continuous Damage Mechanics (CDM) is a more rational approach. PMCs experience damage and unrecoverable deformations similar to plasticity. CDM can be applied to the constituents (fiber, matrix, interphase) at the micro-scale [1-3]. In principle, these models should need a small number of material parameters because each phase is isotropic [3]. However, the constituents cannot be tested in isolation, so they must be tested as part of a lamina. It is difficult to design material tests at the mesoscale (lamina) level that reveal the material parameters in the constituents. One such micro scale level model is presented in [2]. The micro scale level model in [3] includes a detailed identification of material parameters in terms of lamina level tests. From a computational point of view, micro scale-level models are expensive, because they require an excellent micro mechanics model in order to assemble the contributions of the constituents into the lamina behavior. Furthermore, accurate micro mechanics is needed to decompose the meso scale level stress and strain among the constituents. Ref. 3 uses the periodic microstructure model (PMM) from [4], which is very accurate.

A simpler approach is to work directly at the mesoscale modeling the behavior of a homogeneous, orthotropic lamina. The material is assumed to be orthotropic and not transversely isotropic because even isotropic materials become orthotropic after damage [5]. Therefore, use of scalar damage is not appropriate, although it has been done [6]. The simplest yet realistic representation of damage is a second order diagonal tensor with principal directions aligned with the material directions [7]. This works well for PMC because the fiber direction dominates the response; all micro cracks are thus oriented in three perpendicular planes coinciding with the material directions. Any more generality yields models too complex to be practical.

A simple meso scale level model of damage and plasticity is presented in [8]. It works only for plane stress without inter-laminar damage. Its main drawback is its cumbersome identification. In order to identify the material parameters, one has to test a $[+/-67]_S$ laminate, which is not standard. Furthermore, the model does not necessarily predict lamina failure in agreement with any failure criteria such as Tsai-Wu.

In order to address these shortcomings, a new damage constitutive equation is presented in [7]. Then, Ref. [9] extended the damage model of [7] to laminates, performed identification of several PMC materials from published data, and validated the model with additional data not used in the identification process. Later, Ref. [10] added plasticity to the model, identified new materials and further validated the plasticity and the damage portions of the model with new data. The analysis is performed for a lamina in [7], and for laminates in [9-10] using CLT. Then, Lonetti et al. [11] added inter-laminar effects. A finite element formulation of the 3D damage model of [11] is presented and implemented here as a user material model within ANSYS in order to solve more complex laminated problems with general boundary conditions and including the effect of geometrical non linearity.

FINITE ELEMENT FORMULATION

A displacement-based finite element formulation is used. The body of a laminate is represented by a series of layers with different thickness and orientations. Two reference systems, global (x_i, i=1..3) and material (e_i, i=1..3) are used. The local reference axis e_1 is aligned with the fibers direction, e_3 points through the thickness of the laminate, and e_2 lays on the mid-surface of the layer and is perpendicular to e_1 and e_3 ($e_2 = e_3 \times e_1$).

Considering a body B, in which the internal stresses σ, the distributed load *q*, and the concentrated loads *f* constitute an equilibrated system, applying an arbitrary virtual displacement pattern δu^* compatible with the internal strain $\delta\varepsilon^*$, the principle of virtual displacement can be written as

$$\int_V \delta\varepsilon^{*T}\sigma dV - \int_S \delta u^{*T} q dS - \sum_{i=1}^{n_f} \delta u_i^T f_i = 0 \quad , \qquad \textbf{(1)}$$

where n_f is the number of the concentrated loads. Introducing the shape functions *N* and nodal displacement *d* and using the finite element discretization process, Eq.(1) becomes

$$\delta d^T \left(\int_V B^T \sigma dV - \int_S N^T q dS - f \right) = 0, \qquad \textbf{(2)}$$

where *S* is the area in the x_1-x_2 plane, and V = [S x *t*], with *t* total thickness of the laminate. To predict the stiffness reduction, an incremental step-by-step analysis is adopted. For a load increment, Eq.(2) becomes

$$\int_V B^T \Delta\sigma dV - \int_S N^T \Delta q dS - \sum_{i=1}^{n} \Delta f = 0 \qquad (3)$$

where $\Delta\sigma$ represents the stress increment. The damaged stiffness *E* at the current increment can be determined directly from the constitutive equations (Eq. 42-43) as

$$\dot{\sigma} = \frac{\partial\sigma}{\partial\varepsilon}\dot{\varepsilon} + \frac{\partial\sigma}{\partial D}\dot{D} = E\dot{\varepsilon} \qquad \textbf{(4)}$$

Substituting Eq. (4) into Eq.(3), we get

$$\left[K_{epd}\right]\left[\Delta \underset{\sim}{u}\right]=\left[\Delta F\right] \tag{5}$$

where the stiffness matrix and the load vector are

$$\begin{aligned}\left[K_{epd}\right]&=\int_V\left[B^T E^{epd} B\right]dV\\ \left[\Delta F\right]&=\int_S N^T \Delta q dS+\Delta f\end{aligned} \tag{6}$$

The incremental form of the governing equation can be written as

$$\left[K_{NL}^M+K_{NL}^G\right]\left[\Delta u\right]=\Delta F \tag{7}$$

where Δu is the incremental displacement, K_{NL}^M is the non linear material tangent stiffness matrix, K_{NL}^G is non linear geometrical contribution, and ΔF is out balance force.

Damage is monitored at the Gauss integration points. The following algorithm is used to integrate numerically the rate equations. First, compute the strain and stress increment Δε, Δσin the local coordinate system for each lamina at each gauss point

$$\left[\Delta\varepsilon\right]_L=T_k\left[\Delta\varepsilon\right]_G \quad ; \quad \left[\Delta\sigma\right]_L=T_k\left[\Delta\sigma\right]_G \tag{8}$$

where the T_k is a coordinate matrix transformation [1]. Subscripts L, G, indicate local and global coordinates, respectively. An elastic predictor and inelastic corrector scheme is used to determine the effect of a small strain increment $\Delta\varepsilon$. In this way the initial increment is purely elastic. Damage is evaluated in order to check if the inelastic effects grow. There are two possible cases, elastic behavior ($g^d<0$) or damage evolution ($g^d\geq 0$). The evolution of damage variables is subjected to the return-mapping algorithm. In this way, the damage domain is linearized to the first order as

$$g^d \cong g^d{}_{i+1}+\left.\frac{\partial g^d}{\partial Y}\right|_{i+1}^k\left(Y-Y_{i+1}^k\right)+\left.\frac{\partial g^d}{\partial \gamma}\right|_{i+1}^k\left(\gamma-\gamma_{i+1}^k\right) \tag{9}$$

where the subscript (i+1) indicates load step, while superscript (k) represent the iteration number. The thermodynamic forces (Y,γ) and the effective stress $\overline{\sigma}$, can be expressed by using the constitutive and evolution equations in terms of the kinematic quantities (D,ε) and the damage multiplier as

$$
\begin{aligned}
&\left(Y_{i+1}^{k+1}-Y_{i+1}^{k}\right)=\left.\frac{\partial Y}{\partial D}\right|_{i+1}^{k}\left(D_{i+1}^{k+1}-D_{i+1}^{k}\right)+\left.\frac{\partial Y}{\partial \varepsilon}\right|_{i+1}^{k}\left(\varepsilon_{i+1}^{k+1}-\varepsilon_{i+1}^{k}\right)\\
&\left(\gamma_{i+1}^{k+1}-\gamma_{i+1}^{k}\right)=\left.\frac{\partial \gamma}{\partial \delta}\right|_{i+1}^{k}-\Delta\lambda^{d}\\
&\left(\overline{\sigma}_{i+1}^{(k+1)}-\overline{\sigma}_{i+1}^{(k)}\right)=M^{-1}\left(\sigma_{i+1}^{(k+1)}-\sigma_{i+1}^{(k)}\right)\\
&\left(\sigma_{i+1}^{(k+1)}-\sigma_{i+1}^{(k)}\right)=\left[E\left(D\right)\left(\varepsilon_{i+1}^{k+1}-\varepsilon_{i+1}^{k}\right)+\left.\frac{\partial \sigma}{\partial D}\right|_{i+1}^{k}\left(D_{i+1}^{k+1}-D_{i+1}^{k}\right)\right]\\
&\left(D_{i+1}^{k+1}-D_{i+1}^{k}\right)=\Delta\lambda^{d}\left.\frac{\partial f^{d}}{\partial Y}\right|_{i+1}^{k}\left(\varepsilon_{i+1}^{(k+1)}-\varepsilon_{i+1}^{(k)}\right)
\end{aligned}
\tag{10}
$$

In the general case when damage grows, Eqs (10) leads to a linear system that can be solved for the damage multiplier $\Delta\lambda^{d}$. The last step is to check if the damage state variables D_i have reached the critical values D_i^{CR}. When a damage component exceeds the critical value, it signals the appearance of a macro-crack. Therefore, the damage component is set to nearly one ($D_i=1$) to enforce total reduction of stiffness at the Gauss point.

USER DEFINED MATERIAL MODEL

In order to incorporate material non-linearity, a user-defined subroutine is written in Fortran and linked with ANSYS. In the process of linking, a customized ANSYS executable file is obtained which is used for the analysis. The procedure for getting the executable file [12] is as follows: A new directory is created in the drive where ANSYS is installed. The following files are then copied to the new directory from the \custom\user sub directory in ANSYS: Anscust.bat, Makefile, Ansysex.def. The Fortran files are then compiled and linked with ANSYS by running the Anscust.bat file. The procedure will load object files and library files after the compilation and a new executable ANSYS file will be created and will reside in the new directory.

Continuous damage mechanics coupled with thermodynamics is used in order to predict the inelastic behavior of a material. In this case, a set of internal variables is used to describe the damage behavior. The damage model used for modeling the user material is based on available data [7,9-11]. The simplicity of the model lies in the fact that only a few parameters are required to model non-linearity and they can be obtained from standard tests. The model predicts the non-linear effects as a reduction of stiffness and increments of damage. It requires 20 user constants, including five initial transversely isotropic properties, three state variables d_1, d_2 and d_3, also called damage variables, and 12 material parameters. The damage variables are: the damage in fiber direction d_1, the damage in transverse direction d_2, and the damage in the direction perpendicular to the fiber d_3.

The 12 material parameters that are required for the damage model are as follows:

a. Six internal parameters J_{11}, J_{22}, J_{33}, H_1, H_2, H_3 that are univocally defined in terms of experimental material properties.
b. Three critical damage values in tension and compression along the fiber and transverse directions: D_{1TCR}, D_{1CCR}, D_{2TCR}.
c. Three damage threshold and damage evolution parameters: γc_1, and c_2.

Internal Material Constants

The internal material constants (J_{11}, J_{22}, J_{33}, H_1, H_2, H_3) are computed a priori and do not change during the course of the analysis. They are defined in term of the following experimental properties.
a. Critical damage values in tension (D_{1TCR}, D_{2TCR}) and compression (D_{1CCR})
b. The stiffness values (E_1, E_2, G_{12}, G_{23}, ν_{12})
c. The strength values in tension (F_{1t}, F_{2t}), compression (F_{1c}) and shear (F_4, F_5, F_6)
d. Damaged shear modulus at failure (G_{12}^*, G_{13}^*, G_{23}^*)

The internal constants are defined by fourth and second order tensors J and H. They appear in the formulation of the damage surface g

$$g = \left(Y_{ij} \;\; J_{ijhk} Y_{hk}\right)^{1/2} + \left(\left|H_{ij} \;\; Y_{ij}\right|\right)^{1/2} - \gamma(\delta) - \gamma_0 \qquad \textbf{(11)}$$

in thermodynamic force space Y

$$Y_{ij} = -\frac{1}{2}\frac{\partial\left(E_{pqrs}\varepsilon_{pq}\varepsilon_{rs}\right)}{\partial D_{ij}} \qquad \textbf{(12)}$$

In stress space, Eq. (11) represents the Tsai-Wu surface at failure with

Y = Thermodynamic force tensor dual to the damage tensor D
J, H = Internal material constants
$\gamma(\delta)$ = Damage evolution variable
γ_0 = Damage threshold representing the initial size of the damage surface

No damage occurs until the thermodynamic force Y reaches the damage surface. For undamaged material $\gamma = 0$ and g has the shape of the Tsai-Wu surface.
At failure, $\gamma^* + \gamma_0 = 1$ and the shape and size of g matches the Tsai-Wu surface, where γ^* represents the value of γ at failure. Comparing the g-surface with the Tsai-Wu surface at failure, we arrive at a linear system of equations for determination of the J and H tensors as follows.

Calculation of J_{11}, H_1

When the composite lamina is subjected to uniaxial load in the longitudinal direction, all stress components other than σ_1 are zero. Therefore (Eq .11) reduces to

$$g = \sqrt{J_{11}}\frac{\overline{C_{11}}}{\Omega_1^6}\sigma_1^2 + \sqrt{\left|H_1\right|\frac{\overline{C_{11}}}{\Omega_1^6}}\sigma_1 - \left(\gamma + \gamma_0\right) \qquad (13)$$

with the integrity tensor given by

$$\Omega = \sqrt{I - D} \tag{14}$$

where

$\overline{C}$ = Compliance tensor of the undamaged material

Ω = Integrity tensor

D = Damage tensor

At failure, the damage variables reach the critical values (D_{1t}, D_{1c}). If F_{1t} represents the tensile strength and F_{1c} the compressive strength, (Eq. 13) becomes

$$\sqrt{J_{11}}\frac{\overline{C_{11}}}{\Omega_{1t}^6}F_{1t}^2 + \sqrt{|H_1|\frac{\overline{C_{11}}}{\Omega_{1t}^6}F_{1t}} = \left(\gamma^* + \gamma_0\right) \tag{15}$$

$$\sqrt{J_{11}}\frac{\overline{C_{11}}}{\Omega_{1c}^6}F_{1c}^2 + \sqrt{|H_1|\frac{\overline{C_{11}}}{\Omega_{1c}^6}F_{1c}} = \left(\gamma^* + \gamma_0\right) \tag{16}$$

$$\Omega_{1t} = 1\text{-}D_{1t} \quad \text{and } \Omega_{1c} = 1\text{-}D_{1c} \tag{17}$$

The Tsai-Wu criterion for uniaxial loading in the fiber direction is given by

$$f_1F_{1t} + f_{11}F_{1t}^2 = 1 \quad \text{and} \quad f_1F_{1c} + f_{11}F_{1c}^2 = 1 \tag{18}$$

Hence the right hand side of (Eq.15) and (Eq.16) should equal 1 so that the damage surface matches with the Tsai-Wu surface at failure. The critical damage values are obtained from statistical methods [7]. Then the two equations are solved simultaneously and the values of J_{11} and H_1 are obtained.

Calculation of J_{22}, H_2

When the composite lamina is subjected to transverse uniaxial loading, all the stress components other than σ_2 are zero. At failure, (Eq .11) reduces to

$$\sqrt{J_{22}}\frac{\overline{C_{22}}}{\Omega_{2t}^6}F_{2t}^2 + \sqrt{|H_2|\frac{\overline{C_{22}}}{\Omega_{2t}^6}F_{2t}} = \left(\gamma^* + \gamma_0\right) = 1 \tag{19}$$

$$\Omega_{2t} = 1\text{-}D_{2t} \tag{20}$$

When the lamina is subjected to in-plane shear loading, all the stress components other than σ_6 are zero. At failure, (Eq .11) becomes

$$\sqrt{\frac{J_{11}}{\Omega_{1s}^4} + \frac{J_{22}}{\Omega_{2s}^4}}\frac{2\overline{C_{66}}}{\Omega_{1s}^2\Omega_{2s}^2}F_6^2 + \sqrt{\left|\frac{H_1}{\Omega_{1s}^2} + \frac{H_2}{\Omega_{2s}^2}\right|\frac{2\overline{C_{66}}}{\Omega_{1s}^2\Omega_{2s}^2}F_6} = \left(\gamma^* + \gamma_0\right) = 1 \tag{21}$$

Since the shear response of the lamina does not depend on the sign of the shear stress, the coefficient of the linear term in (Eq.21) should be zero. Therefore we get

$$H_2 = -\frac{\Omega_{2s}^2}{\Omega_{1s}^2}H_1 = -r_{s12}H_1 \;;\; r_{s12} = \frac{\Omega_{2s}^2}{\Omega_{1s}^2} \tag{22}$$

$$\sqrt{\frac{J_{11}r_{s12}}{k_{s12}} + \frac{J_{22}}{k_{s12}r_{s12}}}\frac{2\overline{C_{66}}}{k_{s12}}F_6^2 = \left(\gamma^* + \gamma_0\right) = 1 \;;\; k_{s12} = \Omega_{1s}^2\Omega_{2s}^2 \tag{23}$$

Now k_{s12} can be approximated as the ratio of damaged shear modulus to the undamaged shear modulus [7,9-11]

$$k_{s12} = \frac{G_{12}^*}{G_{12}} \tag{24}$$

Also, it has been experimentally observed that most of the shear damage is in the form of longitudinal cracks rather than the transverse cracks [7] and hence $D_{2s}>D_{1s}$ or from (Eq.12) we obtain the restriction

$$0 < r_{S12} < 1 \tag{25}$$

Substituting Eq. (24) in Eq. (23) and solving Eq. (19, 22, 23) we obtain the values of J_{22} and H_2.

Calculation of J_{33} and H_3

In this case the inter-laminar stresses are taken into consideration. The formulation of equations is similar as that of the in-plane case. When the lamina is subjected to inter-laminar stresses, at failure, (Eq.11) reduces to

$$\sqrt{\frac{J_{11}}{\Omega_{1s}^4} + \frac{J_{33}}{\Omega_{3s}^4}\frac{2\overline{C_{55}}}{\Omega_{1s}^2\Omega_{3s}^2}F_5^2} + \sqrt{\left|\frac{H_1}{\Omega_{1s}^2} + \frac{H_3}{\Omega_{3s}^2}\right|\frac{2\overline{C_{55}}}{\Omega_{1s}^2\Omega_{2s}^2}F_5} = \left(\gamma^* + \gamma_0\right) = 1 \tag{26}$$

$$\sqrt{\frac{J_{33}}{\Omega_{3s}^4} + \frac{J_{22}}{\Omega_{2s}^4}\frac{2\overline{C_{44}}}{\Omega_{3s}^2\Omega_{2s}^2}F_4^2} + \sqrt{\left|\frac{H_3}{\Omega_{3s}^2} + \frac{H_2}{\Omega_{2s}^2}\right|\frac{2\overline{C_{44}}}{\Omega_{3s}^2\Omega_{2s}^2}F_4} = \left(\gamma^* + \gamma_0\right) = 1 \tag{27}$$

Since the shear response does not depend on the sign of the shear stress, the coefficients of the linear term must be zero. Therefore we get,

$$H_3 = -\frac{\Omega_{3s}^2}{\Omega_{1s}^2}H_1 = -r_{s13}H_1 \;;\; r_{s13} = \frac{\Omega_{3s}^2}{\Omega_{1s}^2} \tag{28}$$

$$H_2 = -\frac{\Omega_{2s}^2}{\Omega_{3s}^2}H_3 = -r_{s23}H_3 \;;\; r_{s23} = \frac{\Omega_{2s}^2}{\Omega_{3s}^2} \tag{29}$$

Also, it has been experimentally observed that r_{s13} should be less than 1 [11]. Similar to k_{s12} in (Eq. 24) we have k_{s13} and k_{s23} given by

$$k_{s13} = \Omega_{1s}^2\Omega_{3s}^2 = \frac{G_{13}^*}{G_{13}} \tag{30}$$

$$k_{s23} = \Omega_{2s}^2\Omega_{3s}^2 = \frac{G_{23}^*}{G_{23}} \tag{31}$$

Therefore (Eq. 26) and (Eq. 27) reduce to

$$\sqrt{\frac{J_{11}r_{s13}}{k_{s13}} + \frac{J_{33}}{k_{s13}r_{s13}}\frac{2\overline{C_{55}}}{k_{s13}}F_5^2} = \left(\gamma^* + \gamma_0\right) = 1 \tag{32}$$

$$\sqrt{\frac{J_{22}r_{s23}}{k_{s23}} + \frac{J_{33}}{k_{s23}r_{s23}}\frac{2\overline{C_{44}}}{k_{s23}}F_4^2} = \left(\gamma^* + \gamma_0\right) = 1 \tag{33}$$

Solving (Eq. 32) and (Eq. 33) we obtain the values of J_{33}, H_3. The next step is to determine the evolution or hardening parameters c_1, c_2 and damage threshold γ_0.

Flow and Hardening Rules

A non-associated flow rule is used for the damage model [7,9-11]. The flow potential surface is given by the following equation

$$f = \left(Y_{ij} \;\; J_{ijhk} Y_{hk}\right)^{1/2} - \gamma(\delta) - \gamma_0 \qquad \textbf{(34)}$$

The damage and flow surface expand as a function of evolution variable γ according to the evolution law

$$\gamma = -\frac{\partial \pi}{\partial \delta} = c_1\left(\exp\left(\frac{\delta}{c_2}\right) - 1\right) \qquad \textbf{(35)}$$

where $\pi(\delta)$ is the dissipation energy and c_1, c_2 are material constants, which have to be determined from experimental data. Since the dissipation energy should be convex [7], its second derivative should be positive

$$\pi'' = -\frac{c_1}{c_2}\exp\left(\frac{\delta}{c_2}\right) > 0 \qquad \textbf{(36)}$$

In that case the signs of c_1, c_2 should be different. The flow rule for damage and hardening is given by

$$dD = d\lambda \frac{\partial f}{\partial Y} \quad ; \quad d\delta = d\lambda \frac{\partial f}{\partial \gamma} \qquad \textbf{(37)}$$

where $d\lambda$ is the damage multiplier whose value can be determined from the consistency condition ($g = 0$, $dg = 0$)

$$d\lambda = -\frac{\dfrac{\partial g}{\partial Y}\dfrac{\partial Y}{\partial \varepsilon}}{\left[\dfrac{\partial g}{\partial Y}\dfrac{\partial Y}{\partial D}\dfrac{\partial f}{\partial D} + \dfrac{\partial g}{\partial \gamma}\dfrac{\partial \gamma}{\partial \delta}\dfrac{\partial f}{\partial \gamma}\right]} d\varepsilon \qquad \textbf{(38)}$$

Substituting in (Eq. 37) we obtain

$$dD = -\frac{\dfrac{\partial g}{\partial Y}\dfrac{\partial Y}{\partial \varepsilon}}{\left[\dfrac{\partial g}{\partial Y}\dfrac{\partial Y}{\partial D}\dfrac{\partial f}{\partial D} + \dfrac{\partial g}{\partial \gamma}\dfrac{\partial \gamma}{\partial \delta}\dfrac{\partial f}{\partial \gamma}\right]}\frac{\partial f}{\partial Y} d\varepsilon \qquad \textbf{(39)}$$

The incremental stress- strain relations for damage evolution is given by

$$d\sigma = \frac{\partial \sigma}{\partial \varepsilon} d\varepsilon + \frac{\partial \sigma}{\partial D} dD \tag{40}$$

where ε is the total strain. Substituting dD from (Eq. 39) into (Eq. 40) we get,

$$d\sigma = \left(\frac{\partial \sigma}{\partial \varepsilon} - \frac{\partial \sigma}{\partial D} \frac{\frac{\partial \mathrm{g}}{\partial \mathrm{Y}} \frac{\partial \mathrm{Y}}{\partial \varepsilon}}{\left[\frac{\partial \mathrm{g}}{\partial \mathrm{Y}} \frac{\partial \mathrm{Y}}{\partial \mathrm{D}} \frac{\partial \mathrm{f}}{\partial \mathrm{D}} + \frac{\partial \mathrm{g}}{\partial \gamma} \frac{\partial \gamma}{\partial \delta} \frac{\partial \mathrm{f}}{\partial \gamma} \right]} \frac{\partial \mathrm{f}}{\partial \mathrm{Y}} \right) \mathrm{d}\varepsilon = E_{mnl} d\varepsilon \tag{41}$$

where

$$E_{mnl} = \frac{\partial \sigma}{\partial \varepsilon} - \frac{\partial \sigma}{\partial D} \frac{\frac{\partial \mathrm{g}}{\partial \mathrm{Y}} \frac{\partial \mathrm{Y}}{\partial \varepsilon}}{\left[\frac{\partial \mathrm{g}}{\partial \mathrm{Y}} \frac{\partial \mathrm{Y}}{\partial \mathrm{D}} \frac{\partial \mathrm{f}}{\partial \mathrm{D}} + \frac{\partial \mathrm{g}}{\partial \gamma} \frac{\partial \gamma}{\partial \delta} \frac{\partial \mathrm{f}}{\partial \gamma} \right]} \frac{\partial \mathrm{f}}{\partial \mathrm{Y}} \tag{42}$$

Here E_{mnl} represents the tangent stiffness due to the material non-linearity. When geometrical non-linearity is considered (Eq. 41) is written as

$$d\sigma = \left(E_{mnl} + E_{gnl} \right) d\varepsilon \tag{43}$$

Hardening Parameters and Damage Threshold

The hardening parameters (c_1, c_2) control the damage evolution and the damage threshold (γ_0) represent the initial size of the damage surface. Since the material behavior is highly non-linear for a composite lamina in the in-plane shear mode, the damage is assumed to be notable in this case [7]. Therefore, c_1, c_2 and γ_0 are adjusted to predict the shear response of the lamina subjected to pure shear conditions using Finite Element Analysis.

A single lamina is modeled in ANSYS and subjected to pure shear. The material properties and parameters are input in the ANSYS material model definition. The rear nodes are clamped, and the nodes in the side faces are free to move only in the y-direction. The nodes in the front face of the lamina are given a uniform displacement *v* in the y-direction to simulate the pure shear condition.

The non-linear analysis is run with the user material model, which includes c_1, c_2 and γ_0. During the post processing stage, the sum of the reaction forces F_{xy} and the displacement *v* in the front face of the lamina are recorded for each sub step. The average shear stress is calculated by dividing F_{xy} by the shear area and the shear strain is calculated from the displacement of nodes in the front face of the lamina. The shear stress-strain from the analysis is plotted and compared to the experimental shear response (Fig. 1). If the curves don't match, then the c_1, c_2 and γ_0 values are adjusted and the procedure is repeated until the shear stress-strain matches the experimental shear response.

GEOMETRIC AND FINITE ELEMENT MODELING

Finite element models of the $[0/90]_s$ and $[90/0]_s$ lay-up beams with different aspect ratios (length to height ratio) are developed. Four point bending tests are used in-order to study the effect of aspect ratios on the damage of the beams. Both material and geometric non-linearity are considered for the analysis [14]. Contributions due to in-plane and total damage (both in-plane and inter-laminar damage) are analyzed for each aspect ratio of the beam.

Laminated, rectangular beams with different aspect ratios are modeled in ANSYS using solid elements. Modeling with shell elements is not possible within ANSYS because the code does not supply inter laminar stresses to the user subroutine. Other codes such as ABAQUS and LUSAS were investigated and the same limitation was found. Due to symmetry, only a quarter of the beam is modeled. A rectangular prism is modeled based on the aspect ratio of a beam and then partitioned into 4 layers representing the lay-up configuration with different orientations. Three aspect ratios are considered (a/h =4, 10, and 20). Then, the models are meshed using 3-D 20-noded structural solid elements. The material properties vary with the orientation of the fibers in each layer. Therefore the material orientation option is used in-order to orient the elements, in each layer, according to the lay-up angle. Orthotropic material properties based on available data [7,9-11] are assigned to each layer. Glass/Epoxy and Carbon/Epoxy materials are considered for the analysis. The material properties are shown in Table 1.

Since, only a quarter of the beam is considered, symmetric boundary conditions are given to the nodes at the mid span on the plane YZ and also on the plane of bending XZ (see Fig. 8.3 in [1]). The nodes in the mid-plane at the end of the beam are constrained in the z-direction to simulate the end support. The nodes at a distance of 1/3rd of the length of the beam from the ends, which also belong to the mid surface are given a specified displacement z-direction to simulate the loading. These boundary conditions simulate a four point bending test. The material parameters used for the analysis are shown in Table 2. Each material is analyzed in the $[0/90]_s$ and $[90/0]_s$ lay-ups. The material properties and parameters (with adjusted c_1, c_2 and γ_0) are input in the ANSYS material model definition. The analysis is performed considering (a) In-plane damage only, and (b) Total damage (in-plane and inter-laminar damage).

In-plane Damage Only

In this case, the material parameters J_{33} and H_3 are set to zero so that the inter-laminar damage is turned off. The non-linear analysis is performed on the beam with the optimum number of sub steps. The damage is monitored at the integration points of the elements. When the damage state variables d_i reach the critical values D_i^{cr}, the damage component is set to 1 in order to enforce total stiffness reduction at the Gauss point. During post processing, the sum of reaction forces R_z at the restrained nodes and the deflection w of the end nodes located in the mid-plane are noted. Then the bending stress S is calculated in terms of the reaction R_z output from the analysis as

$$S = \frac{Mc}{I} = \frac{2aR_z}{bh^2} \qquad \textbf{(44)}$$

where a, b, h are the length, width and height of the beam and R_z is the reaction force measured. Then the bending stress is normalized with respect to the transverse tensile strength of the

material F_{2t}. Similarly, the deflection *w* is normalized with respect to the length of the beam *a*. A graph is plotted between S/F_{2t} and *w/a* of the beam. This procedure is repeated for all types of beams (lay-ups and materials). In case the deflection of the beam becomes large (more than 30% of the beam length), geometric non-linearity is considered in addition to the material non-linearity.

Total Damage

In this case, the inter-laminar damage is turned on when actual values of J_{33} and H_3 are input. The rest of the procedure is the same as the previous case. The evolution of the damage variables d_2, d_3 (state variables) is studied. The maximum value of the damage variables is noted at the integration points for each sub-step and a graph is plotted between d_2, d_3 and w/a. The graph gives an indication of the damage growth in the beam.

RESULTS AND DISCUSSION

The damage threshold γ_0 and hardening parameters c_1, c_2, are adjusted to obtain a good correlation between the model predictions and experimental shear stress-strain data, as illustrated in Fig. 1. The results obtained for the Glass/Epoxy composite beam with different aspect ratios (a/h = 4, 10, 20) and lay-up angles ([0/90]s and [90/0]s) are shown in Figs. 2-10. With reference to Fig. 2, the straight line indicates that there is no damage considered for the analysis. This condition is achieved by assigning a large value for the damage threshold (γ_0=1E20), which means that the initial damage surface is very large and hence no damage occurs. The curve below the linear case is the one obtained by considering the in-plane damage only. The main mode of damage is due to d_2, as shown in Fig. 4. When d_2 reaches the maximum value, the solution does not converge and the program stops. This indicates the emergence of a macro crack. The maximum damage value d_2 is 0.59, which exceeds the actual critical damage value D_2^{cr} (Table 2). This is because the damage value 0.59 occurs only in a small region, as it also happens for d_3 (see Fig. 3.) When D_2^{cr} is considered as the limiting damage value, the analysis stops when d_2 reaches D_2^{cr}, as shown in Fig. 2.

The last curve indicates the results for which the total damage is considered (in-plane and the inter-laminar damage). In this case d_3 dominates the damage behavior. This is because the Glass/Epoxy is weak in the inter-laminar direction. This is further shown in Fig. 4 where it can be seen that d_3 is much higher than d_2. The values plotted are the maximum values of the damage variables obtained from the integration points in each sub-step.When D_3^{cr} is considered as the limiting damage value, the analysis stops when d_3 equals D_3^{cr}, as indicated in Fig. 2. The maximum damage value (d_3) is 0.535, which exceeds the actual critical damage value D_3^{cr} (Table 2). The reason being is that d_3 equals 0.535 at a small region, as shown in Fig. 3.

It is worth noting that for the $[0/90]_s$ laminate, the maximum damage in both in-plane (d_2) and total damage (d_3) condition occur in the 90˚ laminate. This is because the 0˚ laminate is subjected to tension at the bottom and compression at the top, where damage is very small because the fibers are strong in the 0˚ direction. At a/h=4 (Fig. 2-4), inter-laminar shear is high and it causes significant out of plane damage d_3. If the model does not consider it (d_3=0), the in-plane damage is underestimated (Fig. 4). When the aspect ratio is 20, the damage d_2 becomes significant in the total damage condition, as shown in Fig. 5-6. The maximum values of d_2 (0.38) and d_3 (0.46) become closer, which means that d_2 begins to dominate the damage in the beam for higher aspect

ratios. This is because inter-laminar shear is less pronounced at high aspect ratios. The effect of damage on deflections (Fig. 5) for a/h=20 is small because the outer layers dominate the stiffness of the beam. Still, the inter-laminar shear strength F_4 of Glass/Epoxy is weak, resulting in significant inter-laminar damage d_3 (Fig. 6).

Similar results can be observed in the $[90/0]_s$ lay-up beams (Fig. 7-10). As a/h increases, the mode of failure changes from d_3 to d_2 (Table 3). In the case of the $[90/0]_S$ laminates, even for the aspect ratio of 10, d_2 starts to dominate the damage in the total damage condition. This is due to the fact that the 90˚ laminate is subjected to a high stress at top and bottom of the beam in the transverse direction where the material is weak. This is the reason why the maximum value of d_2 occurs in the 90˚ laminate and the maximum value of d_3 occurs in the 0˚ laminate. When the aspect ratio is 20, very high deflections in the beam are observed. Hence, geometrical non-linear effects must be considered (Fig. 9). The mode of failure switches to transverse damage d_2 at a/h=20 (Table 3 and Fig. 10).

The inter-laminar damage d_3 dominates the damage in all cases for Carbon/Epoxy composite beam with different aspect ratios (a/h = 4, 10, 20) and lay-up angles ($[0/90]_s$ and $[90/0]_s$). In case of the $[0/90]_s$ lay-up beams (Fig. 11-12), d_2 is significant if d_3 is not modeled (labeled as d_3=0 in the figures), whereas when inter-laminar effects are considered, d_3 controls the damage in the beam. This is due to the fact that the material is strong in the transverse direction and withstands damage due to d_3 even when the aspect ratio increases and the in-plane damage is insignificant.

For Carbon/Epoxy $[0/90]_S$, the dominant mode of failure remains d_3 even at a/h=20 (10-11). The effect of damage on deflections is negligible because the fibers on the outer layers dominate the bending stiffness. In case of the $[90/0]_s$ lay-up beams, similar results as the previous case is obtained except that geometric non linear effects are also considered here due to the large deflection of the beam. Even switching LSS to $[90/0]_S$ the mode of failure remains inter-laminar damage d_3 for Carbon/Epoxy with 4<a/h<20 (Table 4). Significant transverse damage d_2 is accumulated but it is not the critical factor. Neglecting d_3 leads to gross overestimation of the failure load.

CONCLUSIONS

A finite element formulation of continuum damage model that includes inter laminar effects is successfully developed and implemented as a user subroutine in a commercial finite element analysis code. The internal damage parameters are identified from available experimental data. Furthermore, the damage threshold and evolution parameters are identifies from available, experimental shear stress strain data. The finite element formulation and identifies material parameters are then used to investigate the influence of material properties, aspect ratio, laminate stacking sequence, and geometric non linearity on the damage evolution, deflections, and failure of laminated beams under four point loading. Furthermore, the option of neglecting inter laminar damage is shown to lead to misleading predictions of in plane damage evolution and poor predictions of failure load. In case of Glass/Epoxy composite, inter-laminar damage is significant for all $[0/90]_s$ and $[90/0]_s$ beams with low aspect ratios. As the aspect ratio increases, the in-plane damage becomes dominant. In the case of Carbon/Epoxy composite, the inter-laminar damage is dominant for all aspect ratios of the beam.

SIGNIFICANCE – ARMY VALUE

Weapons technology is shifting increasingly towards minimizing mass of defensive weapons as a primary design constraint. This is readily apparent in both tank armor and single soldier armor, not to mention numerous other defense applications. As a part of this new design philosophy, it is clear that significant decreases in armor weight can be achieved by utilizing multi-layered and multi-material structures to defeat offensively fired weapons.

Acknowledgements

The author gratefully acknowledges the technical contributions reported herein by Dr. David Allen (now at the University of Nebraska, Lincoln) and his students and Dr. Ever Barbero of the West Virginia University.

REFERENCES

1. Barbero, E. J. (1999) *Introduction to Composite Materials Design*, Taylor & Francis, Philadelphia, PA.
2. Voyiadjis G. Z., Deliktas B. (2000) A Coupled Anisotropic Damage Model For The Inelastic Response Of Composite Materials, *Comp. Methods in Appl. Mech. Eng*., v183, 159-199.
3. Abdelal, G. F., Caceres, A., Barbero, E. J. A Micromechanics Damage Approach for Fatigue of Composite Materials, *J. Composite Structures*, 56(4) 2002 413-xxx.
4. Luciano, R. and E. J. Barbero, "Formulas for the Stiffness of Composites with Periodic Microstructure," *Int. J. of Solids Structures*, 31(21), 2933-2944, (1995).
5. Cordebois J.L., Sirodoff F.(1979) Damage-induced elastic anisotropyMechanics of Behavior of Anisotropic Solids/N295 *Comportement Mechanique Des Solides Anisotropes*, Martinus Nijhoff Publisher, pp.19-22
6. Chaboche J. L. (1993) Development of CDM for Elastic Solids Sustaining Anisotropic and Unilateral Damage, *Int. J. of Damage Mechanics*, v2(4), 311-317.
7. Barbero, E. J. and DeVivo, L. (2001) A Constitutive Model for Elastic Damage in Fiber-Reinforced PMC Laminae, *J. of Damage Mechanics*, 10(1) 73-93.
8. Ladeveze P., LeDantec E. (1992) Damage Modelling of the Elementary Ply for Laminated Composites, *Composites Science and Technology*, v43, 257-267.
9. Barbero, E. J. and Lonetti, P. (2001) Damage Model for Composites Defined in Terms of Available Data, *Mechanics of Composite Materials and Structures*, 8(4), 299-316.
10. Barbero E.J., Lonetti P. (2002) An Inelastic Damage Model for Fiber Reinforced Laminates, *Journal of Composite Material*, 36(8): 941 – 962.
11. Lonetti, P., R. Zinno, and F. Greco, and Barbero, E. J., (2003) Interlaminar Damage Model For Polymer Matrix Composites, *J. Composite Materials*, 37(15), 1485-1504, 08/2003.
12. ANSYS User Manual, Ansys Inc., Washington, PA.
13. Krajcinovic D. (1996) *Damage Mechanics*, North Holland, Amsterdam, Holland.
14. Reddy, J. N., *Mechanics of Laminated Composite Plates and Shells*, Second Edition, CRC Press, Boca Raton, FL, 2004.

Table 1. Material properties of Glass/Epoxy and Carbon/Epoxy

Property	Glass/Epoxy (V_f = 52%)	Carbon/Epoxy (V_f = 62%)
E_1 (MPa)	36200	131300
E_2 (MPa)	8100	10800
G_{12} (MPa)	3200	5200
G_{13} (MPa)	1500	7100
ν_{12}	0.23	0.29
F_{1t} (MPa)	932	2100
F_{1c} (MPa)	370	1080
F_{2t} (MPa)	42	80
F_4 (MPa)	35	72
F_5 (MPa)	50	70
F_6 (MPa)	50	70
G_{12} damaged (GPa)	2700	2258
G_{13} damaged (GPa)	1299	3083
G_{23} damaged (GPa)	1299	3083

Table 2. Material Parameters for the damage model

Property	Glass/Epoxy	Carbon/Epoxy
J11	0.531e-2	0.1897e-2
J22	0.226	0.287e-1
J33	0.2009	0.534e-1
H1	0.681e-1	0.2571e-1
H2	-0.1445e-1	-0.807e-2
H3	0.592e-1	0.8018e-2
k_{s12}	0.866	0.434
k_{s13}	0.866	0.434
k_{s23}	0.866	0.434
r_{s12}	0.212	0.314
r_{s13}	0.8703	0.311
r_{s23}	4.105	0.992
c_1	0.22	0.045
c_2	-0.3	-0.625
γ_0	0.015	0.07
D_1^{cr}	0.1161	0.1161
D_2^{cr}	0.5	0.5
D_3^{cr}	0.5	0.5

Table 3. Failure stress S/F2t and mode of failure for Glass/Epoxy

Laminate stacking sequence	a/h	S/F2t		Mode	At Failure
		$d_3=0$	$d_3\neq0$		
$[0/90]_s$	4	1.57	1.22	d_3	$d_2=0.243$
	10	4.78	3.61	d_3	$d_2=0.252$
	20	10.00	7.76	d_3	$d_2=0.375$
$[90/0]_s$	4	4.12	1.01	d_3	$d_2=0.204$
	10	5.04	2.91	d_3	$d_2=0.493$
	20	3.45	1.79	d_2	$d_3=0.283$

Table 4. Failure stress S/F2t and mode of failure for Carbon Epoxy

Laminate stacking sequence	a/h	S/F2t		Mode	At Failure
		$d_3=0$	$d_3\neq0$		
$[0/90]_s$	4	1.61	0.69	d_3	$d_2=0.0058$
	10	5.30	2.12	d_3	$d_2=0.0061$
	20	11.42	5.68	d_3	$d_2=0.0069$
$[90/0]_s$	4	5.63	0.50	d_3	$d_2=2.4E-6$
	10	5.53	1.67	d_3	$d_2=0.2271$
	20	3.20	2.00	d_3	$d_2=0.3694$

List of Figures

Fig. 1 Model prediction of the unidirectional shear stress strain curve

Fig. 2 Load-deflection of [0/90]s, Glass/Epoxy, a/h=4.

Fig. 3 Damage evolution d_3 for total damage model of $[0/90]_S$ Glass/Epoxy, a/h=4 at w/a= 0.00913 and normalized stress S/F_{2T}=1.219.

Fig. 4 Damage evolution of [0/90]s, Glass/Epoxy, a/h=4.

Fig. 5 Load-deflection of [0/90]s, Glass/Epoxy, a/h=20.

Fig. 6 Damage evolution for total damage conditions of [0/90]s, Glass/Epoxy, a/h=20.

Fig. 7 Load-deflection of [90/0]s, Glass/Epoxy, a/h=4.

Fig. 8 Damage evolution for total damage conditions of [90/0/]s, Glass/Epoxy, a/h=4.

Fig. 9 Large deflection of [90/0]s Glass/Epoxy, a/h=20.

Fig. 10 Damage evolution for total damage conditions of [90/0/]s, Glass/Epoxy, a/h=20.

Fig. 11 Load-deflection of [0/90]s, Carbon/Epoxy, a/h=20.

Fig. 12 Damage evolution for total damage conditions of [0/90]s, Carbon/Epoxy, a/h=20.

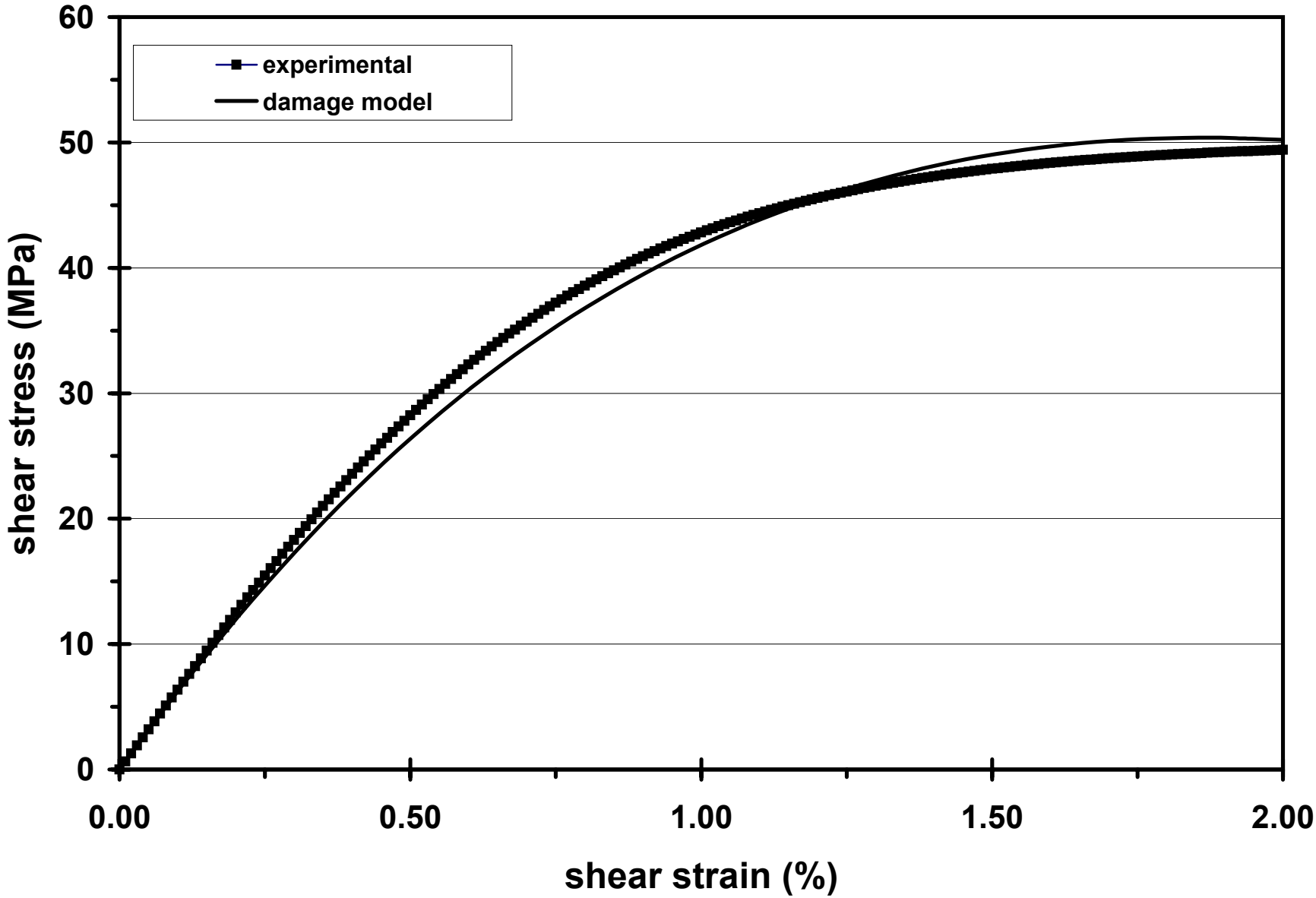
experimental
damage model
shear stress (MPa)
shear strain (%)
0
10
20
30
40
50
60
0.00
0.50
1.00
1.50
2.00

figure 1

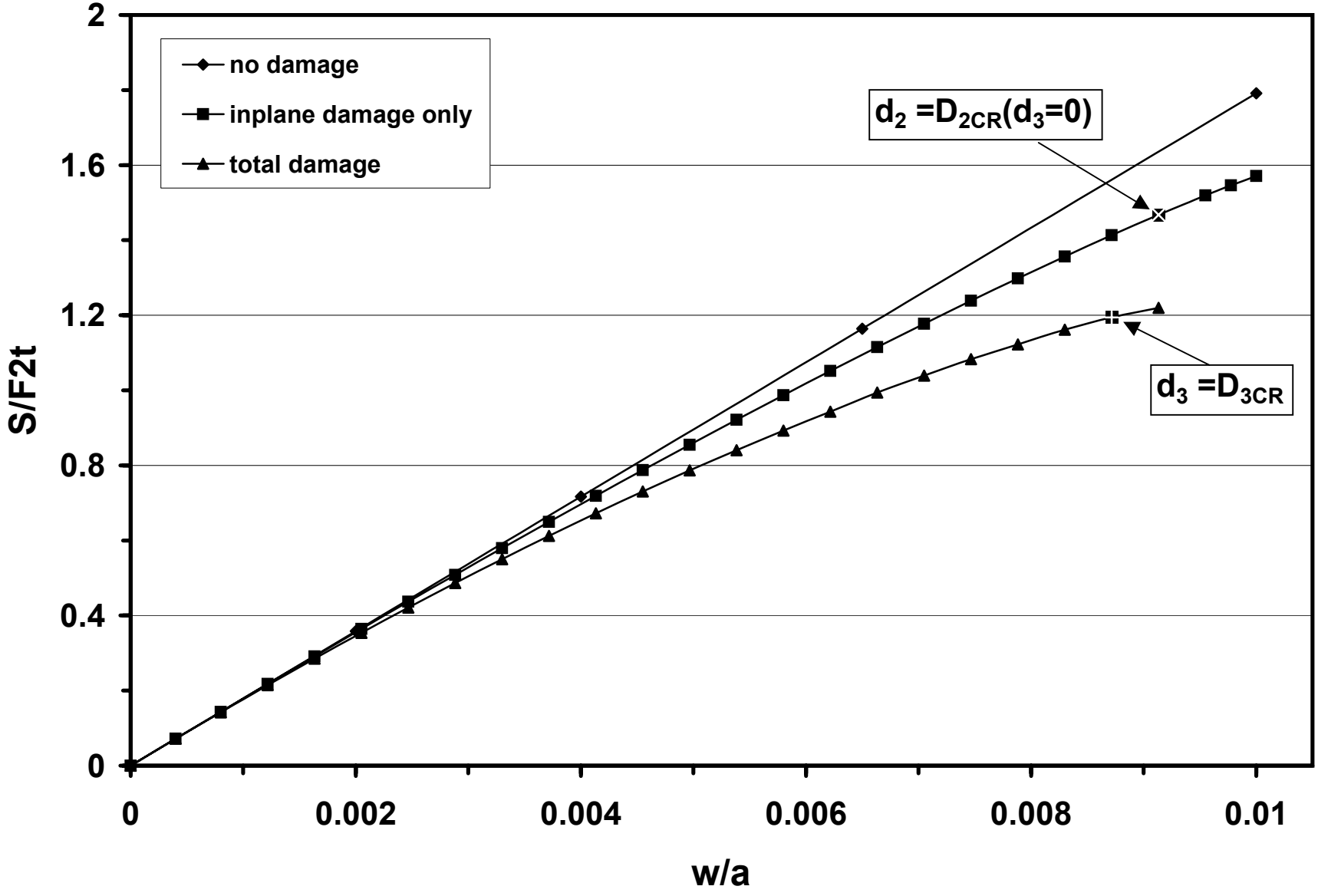
no damage
inplane damage only
total damage
$d_2 = D_{2CR}(d_3=0)$
$d_3 = D_{3CR}$
S/F2t
w/a
0
0.4
0.8
1.2
1.6
2
0
0.002
0.004
0.006
0.008
0.01

figure 2

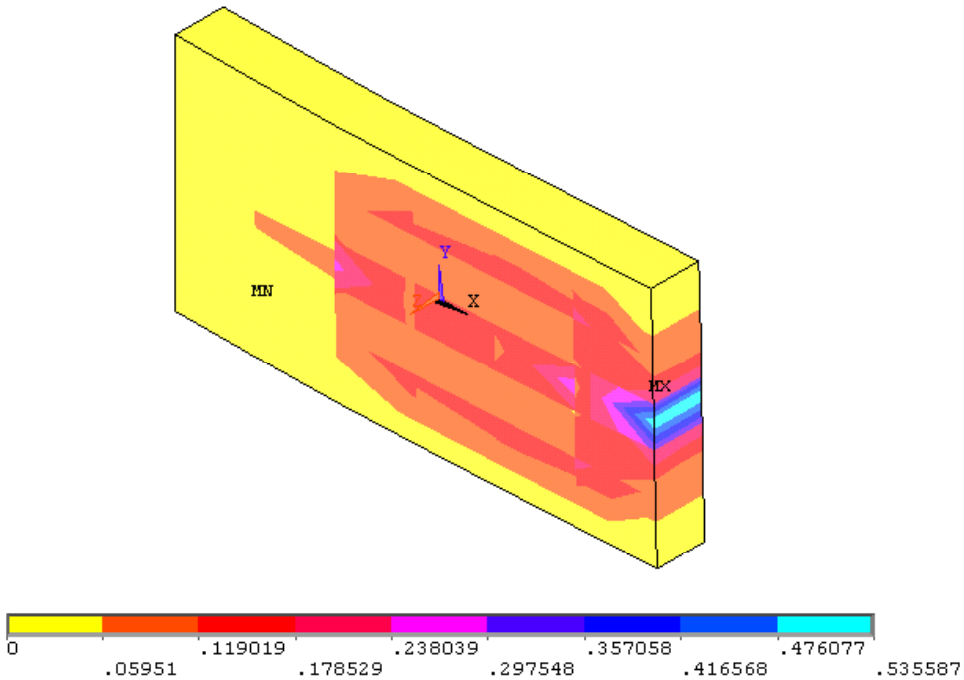

Fig. 3 Damage evolution d_3 for total damage analysis of $[0/90]_S$ Glass/Epoxy, a/h=4, at w/a= 0.00913 and normalized stress S/F_{2T}=1.219

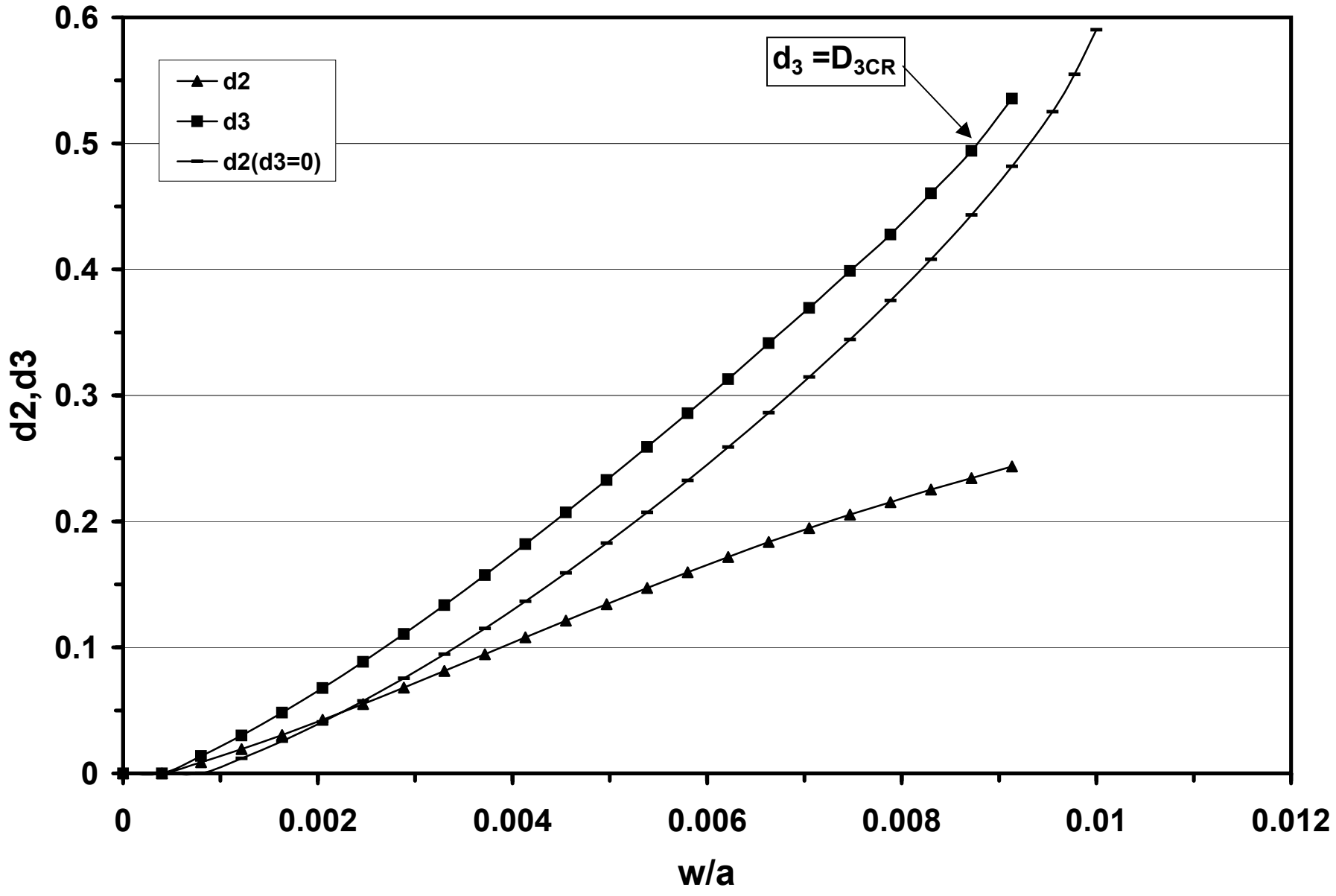
0.6
0.5
0.4
0.3
0.2
0.1
0
d2,d3
d2
d3
d2(d3=0)
d3 =D3CR
0
0.002
0.004
0.006
0.008
0.01
0.012
w/a

figure 4

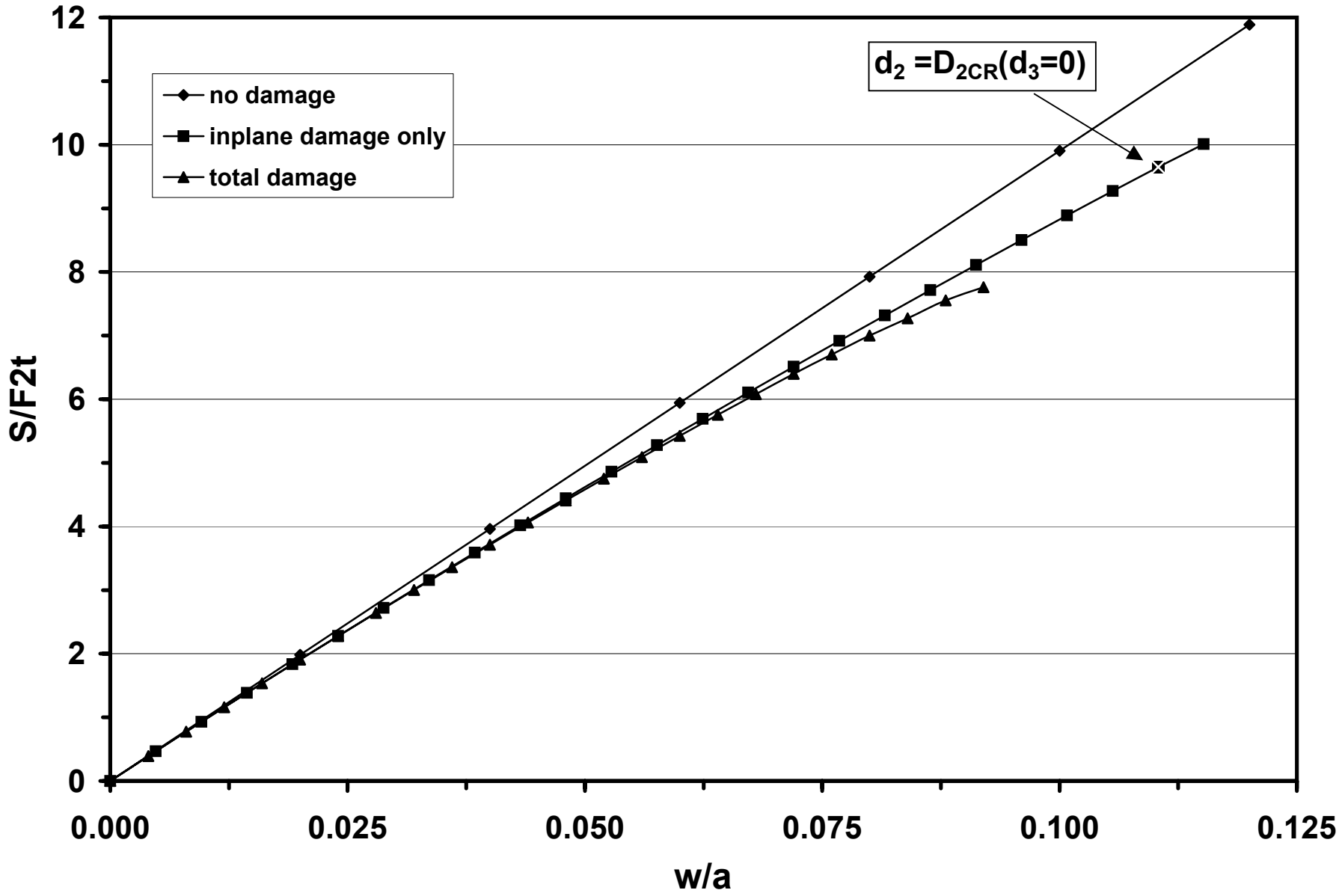
12
10
8
6
4
2
0
S/F2t
0.000
0.025
0.050
0.075
0.100
0.125
w/a
no damage
inplane damage only
total damage
d2 =D2CR(d3=0)

figure 5

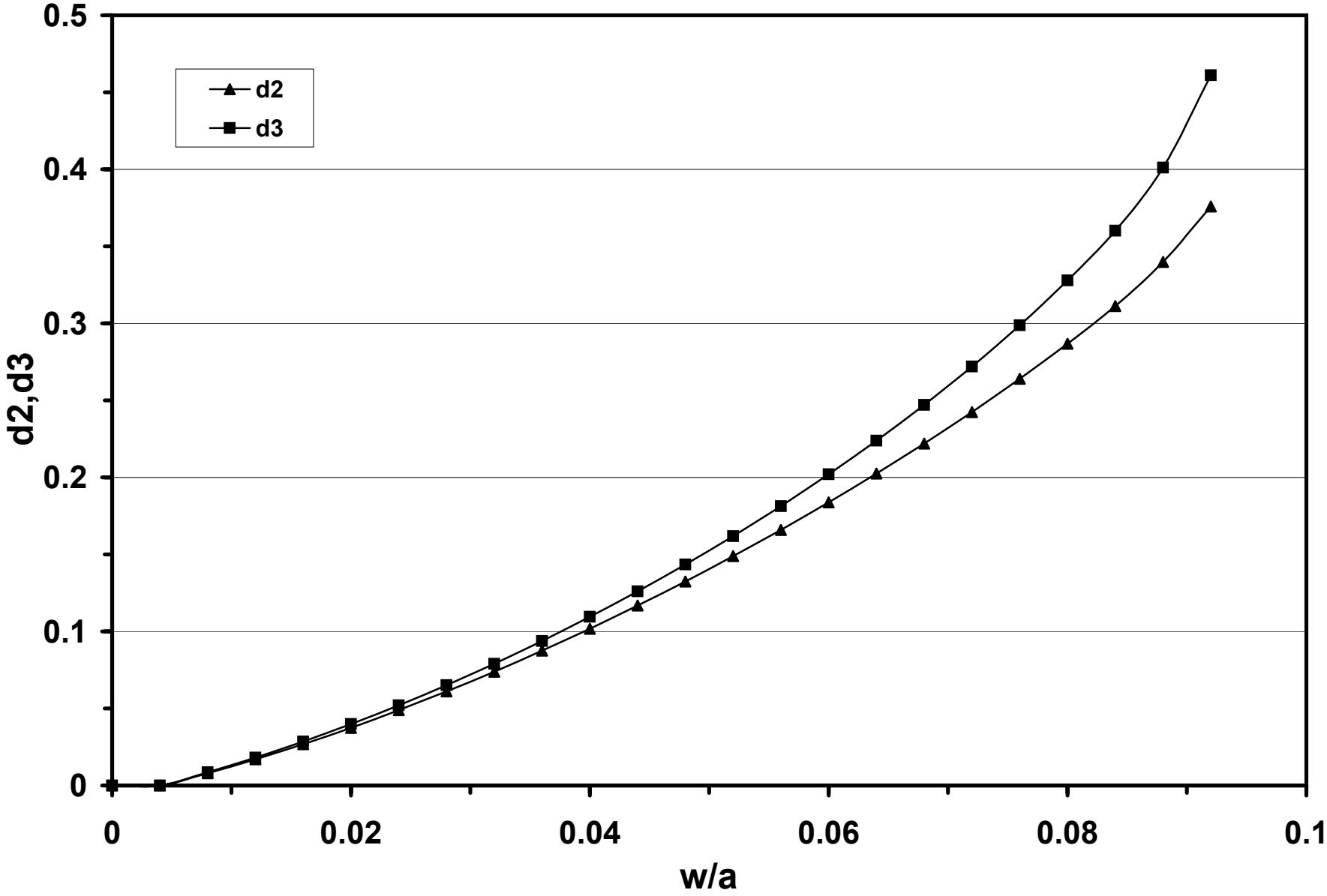

figure 6

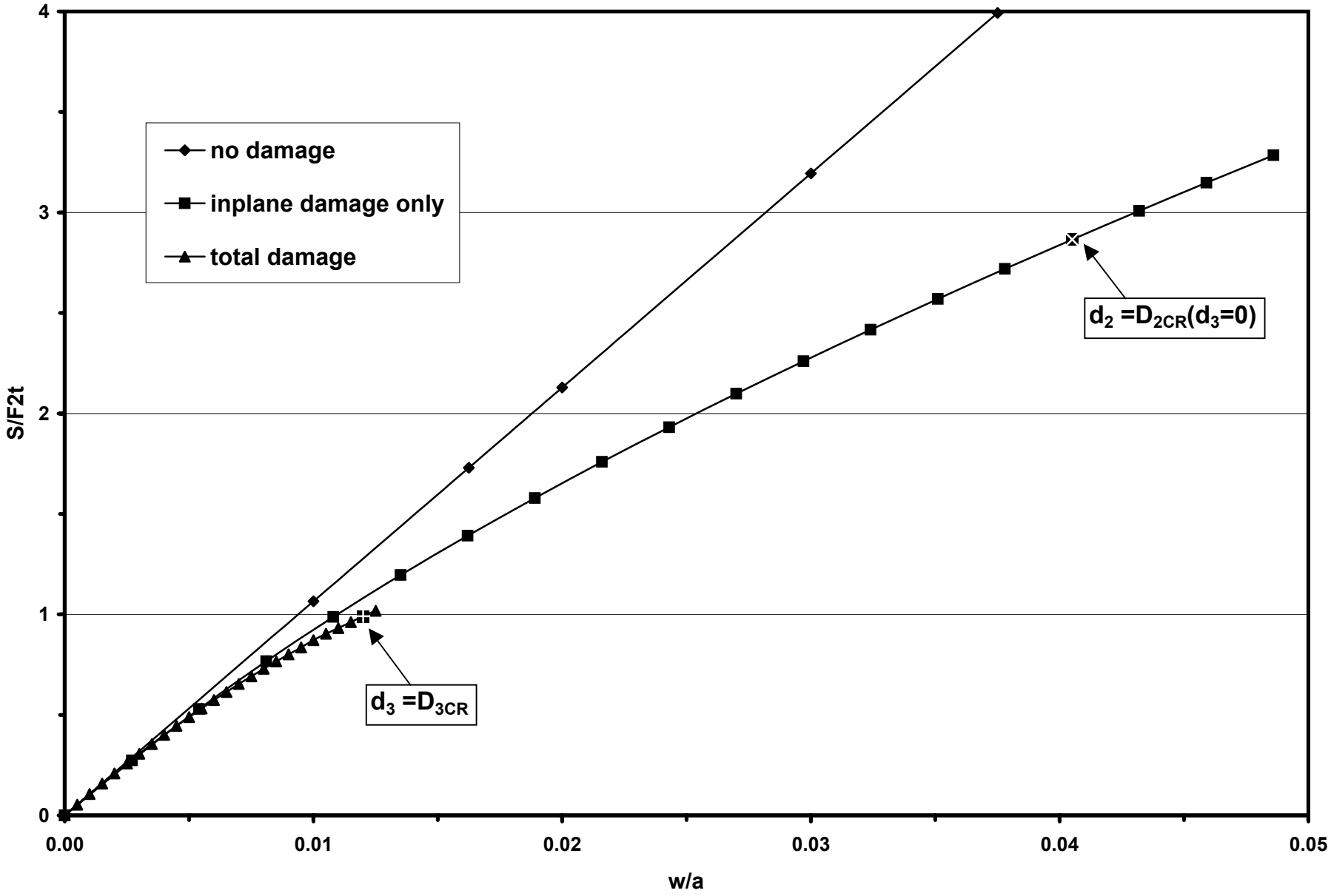
no damage
inplane damage only
total damage
$d_2 = D_{2CR}(d_3=0)$
$d_3 = D_{3CR}$
S/F2t
w/a
0
1
2
3
4
0.00
0.01
0.02
0.03
0.04
0.05

figure 7

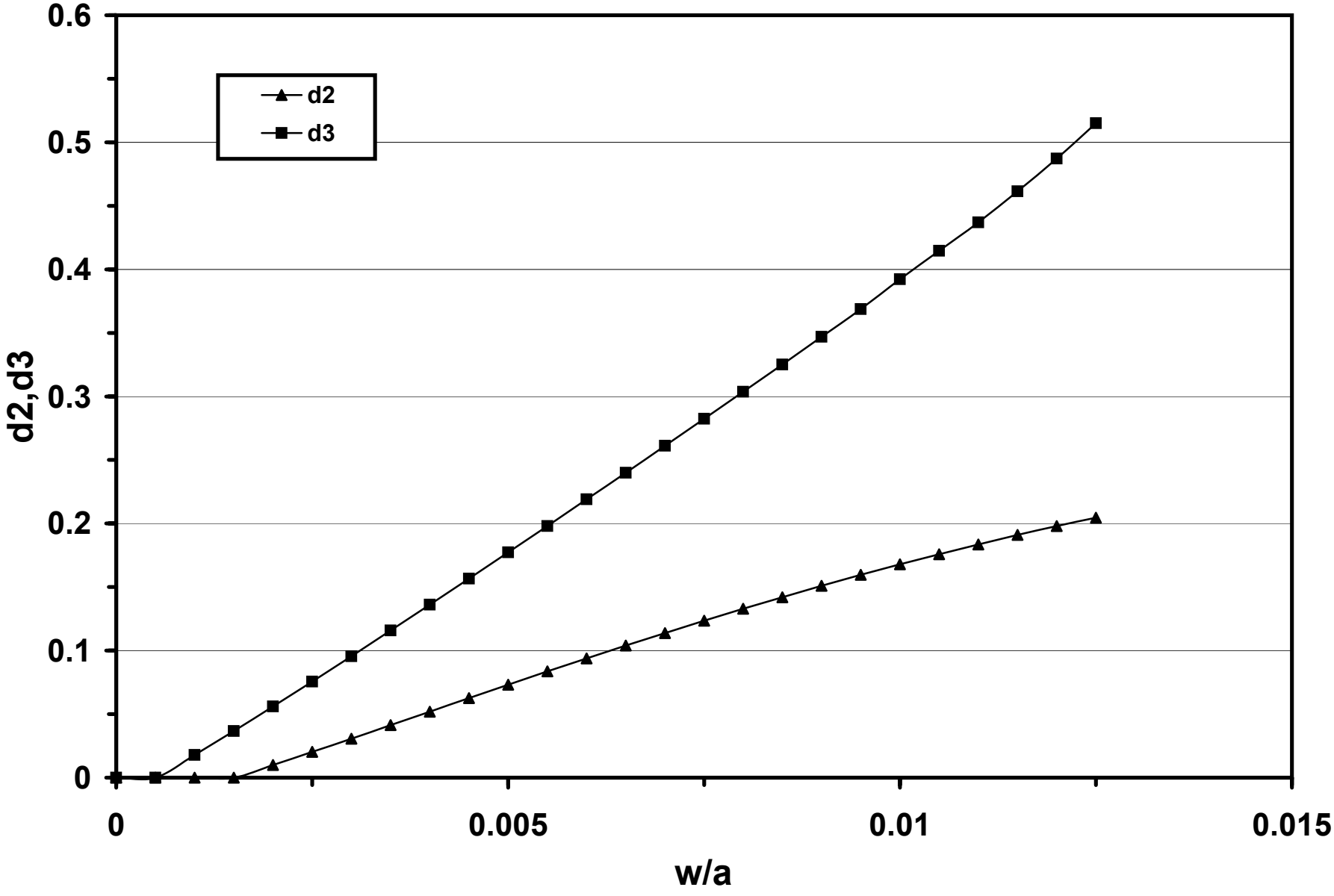

figure 8

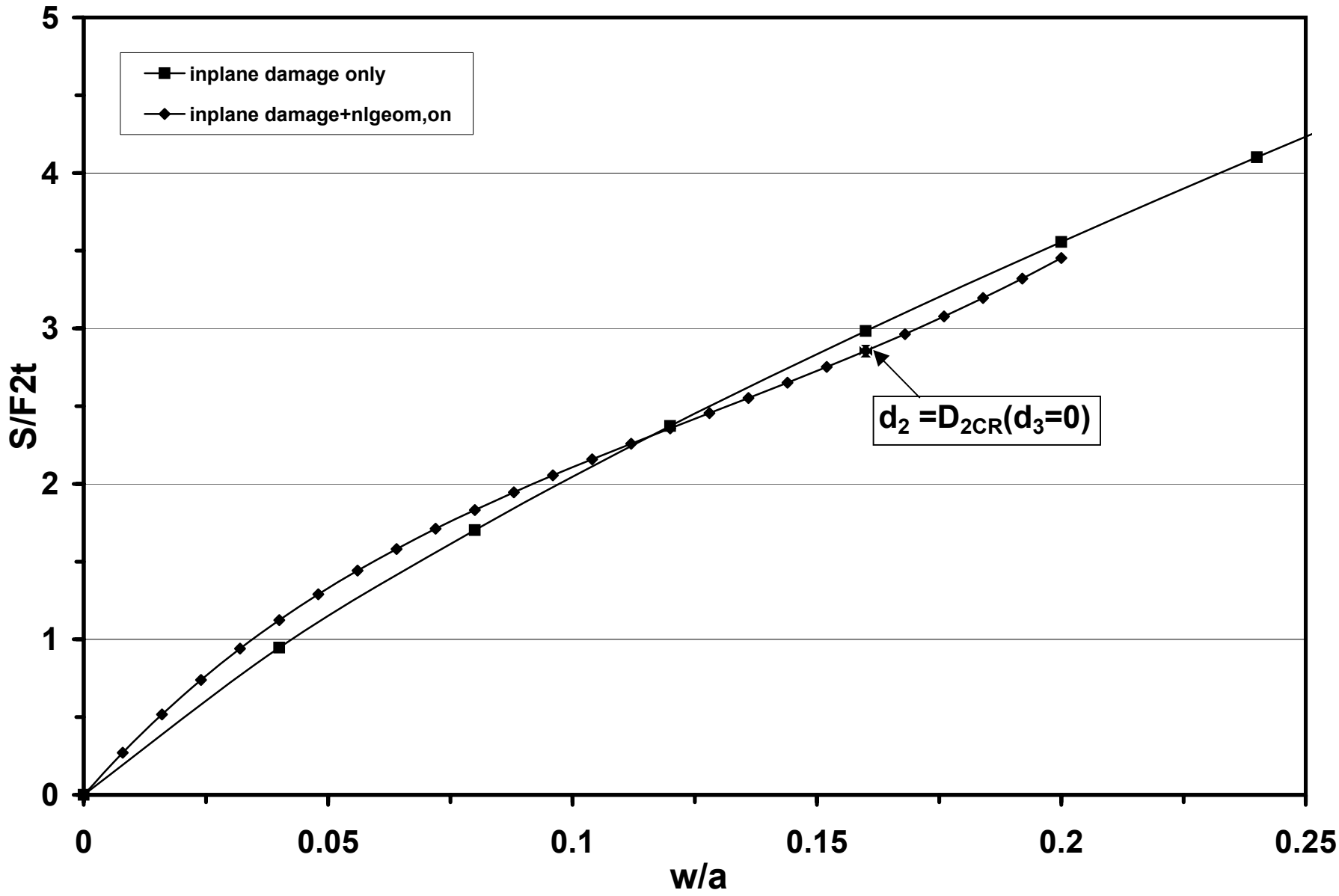
inplane damage only
inplane damage+nlgeom,on
$d_2 = D_{2CR}(d_3=0)$
S/F2t
w/a
0
1
2
3
4
5
0
0.05
0.1
0.15
0.2
0.25

figure 9

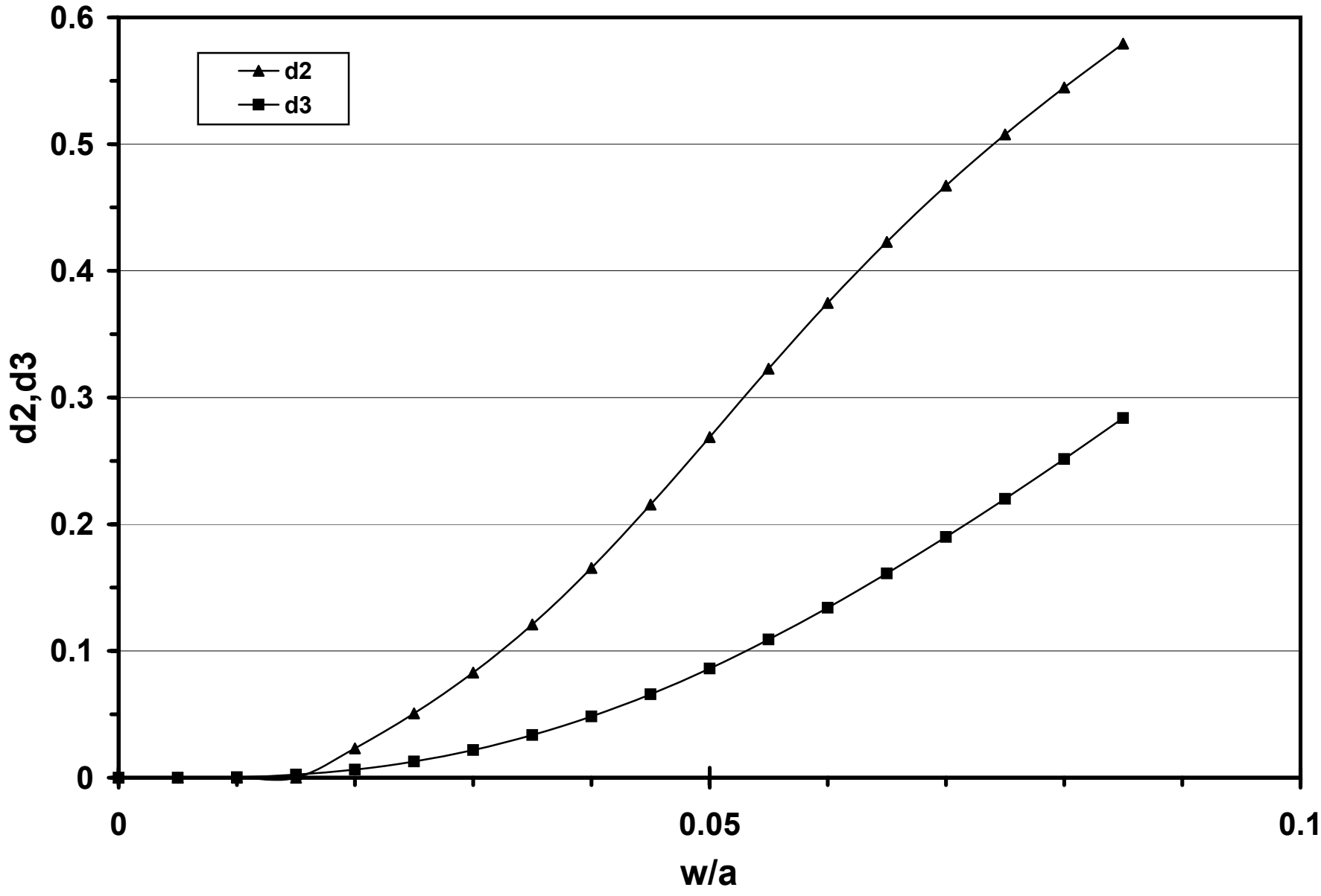

figure 10

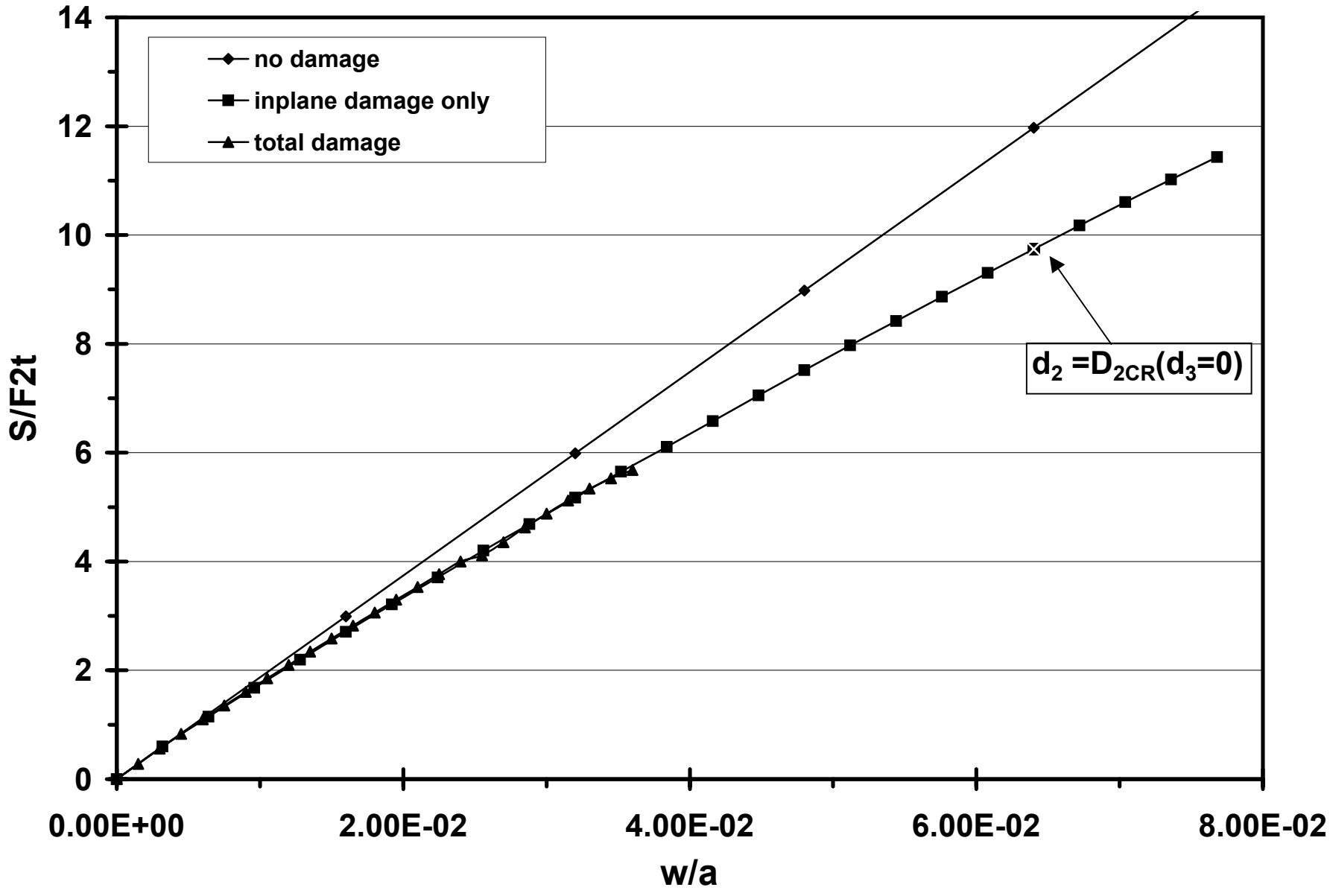
14
12
10
8
6
4
2
0
S/F2t
no damage
inplane damage only
total damage
$d_2 = D_{2CR}(d_3=0)$
0.00E+00
2.00E-02
4.00E-02
6.00E-02
8.00E-02
w/a

figure 11

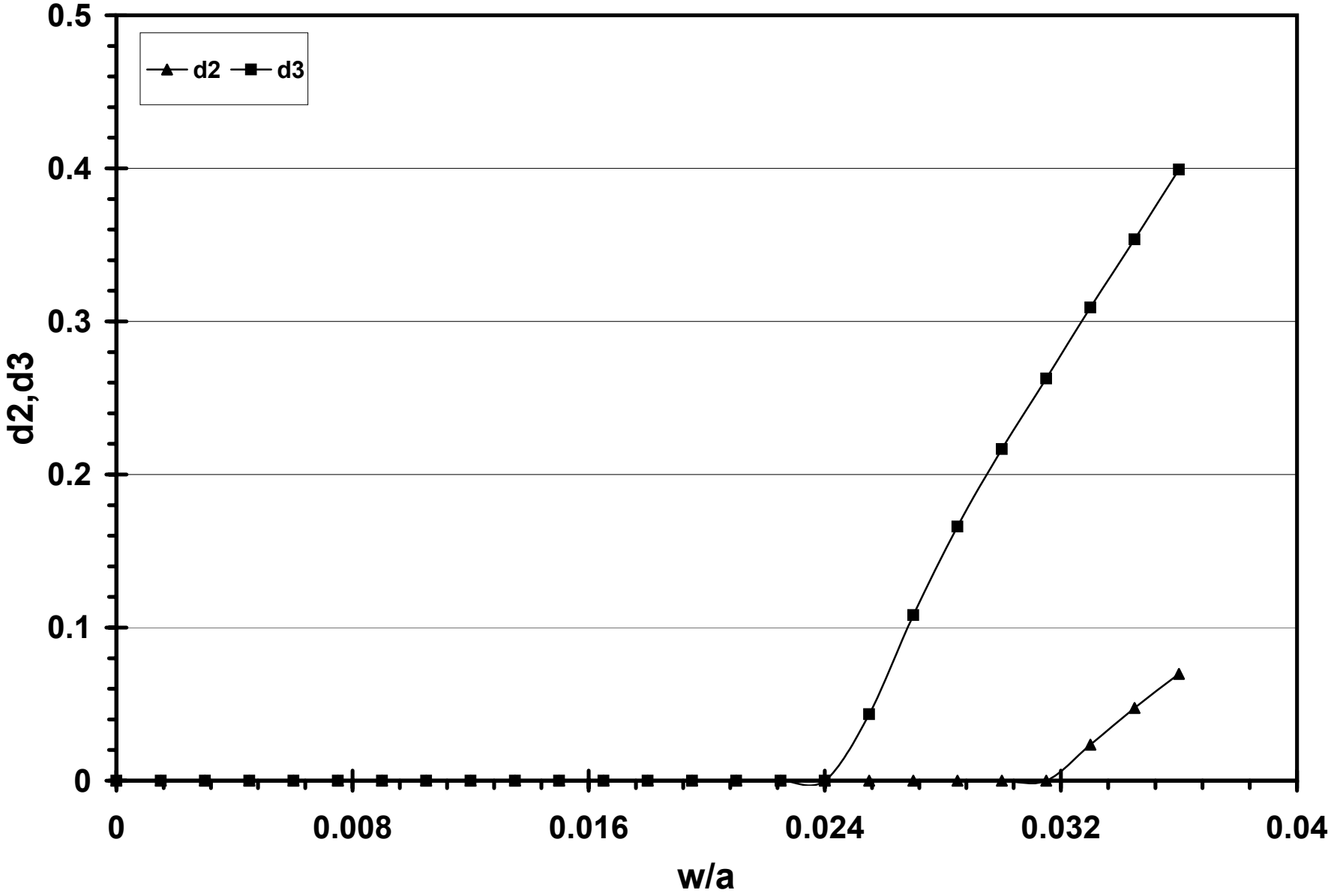

figure 12